

Consistent analysis of the reactions $\gamma p \rightarrow p\eta'$ and $pp \rightarrow pp\eta'$

K. Nakayama^{1,2} and H. Haberzettl^{3,2}

¹*Department of Physics and Astronomy, University of Georgia, Athens, GA 30602, USA*

²*Institut für Kernphysik (Theorie), Forschungszentrum Jülich, D-52425 Jülich, Germany*

³*Center for Nuclear Studies, Department of Physics,*

The George Washington University, Washington, DC 20052, USA

(Dated: 13 January 2004)

The production of η' mesons in the reactions $\gamma p \rightarrow p\eta'$ and $pp \rightarrow pp\eta'$ is described consistently within a relativistic meson exchange model of hadronic interactions. The photoproduction can be described quite well over the entire energy range of available data by considering an S_{11} and a P_{11} resonance, in addition to the t -channel mesonic current. The observed angular distribution is due to the interference between the t -channel and the nucleon resonance s - and u -channel contributions. Our analysis yields positions close to 1650 MeV and 1870 MeV for the S_{11} and P_{11} resonances, respectively. We argue that, at present, identifying these states with the known $S_{11}(1650)$ resonance and the missing P_{11} resonance predicted at 1880 MeV, respectively, would be premature. It is found that the nucleonic current is relatively small and that the $NN\eta'$ coupling constant cannot be much larger than $g_{NN\eta'} = 3$. As for the $pp \rightarrow pp\eta'$ reaction, different current contributions are constrained by a combined analysis of this and the photoproduction reaction. Difficulties to simultaneously account for the 47-MeV and 144-MeV angular distributions measured by the COSY-11 and DISTO collaborations, respectively, are addressed.

PACS numbers: 25.20.Lj, 13.60.Le, 13.75.-n, 14.20.Gk

[nucl-th/0401030—PRC (05/2004)]

I. INTRODUCTION

The study of the intrinsic properties of the η' meson as well as its production processes in elementary particle and hadron physics is of particular interest for various reasons. The properties of η' are largely governed by the dynamics of the QCD $U_A(1)$ axial vector anomaly [1, 2, 3, 4, 5, 6]. Expressed in the (pseudoscalar) quark-flavor basis, the physically observed η and η' mesons may be written as

$$\begin{pmatrix} \eta \\ \eta' \end{pmatrix} = \begin{pmatrix} \cos \alpha & -\sin \alpha \\ \sin \alpha & \cos \alpha \end{pmatrix} \begin{pmatrix} \eta_q \\ \eta_s \end{pmatrix}, \quad (1)$$

where $\eta_s \equiv s\bar{s}$ and $\eta_q \equiv (u\bar{u} + d\bar{d})/\sqrt{2}$ describe the strange and nonstrange quark-antiquark states, respectively. The $U_A(1)$ anomaly mediates η_q - η_s transitions and therefore plays a central role in understanding the η - η' mixing [7]. The mixing angle α is shown to be fairly constant [7, 8], and a weighted average value of $\alpha = 39.3^\circ \pm 1.0^\circ$ has been extracted [9]. Quite recently, the KLOE collaboration [10] has reported a value of $\alpha = 41.8^{+1.9}_{-1.6}^\circ$. As can be seen from Eq. (1), such a value of the mixing angle results in a considerable amount of $s\bar{s}$ in both the η and η' mesons. By contrast, the corresponding mixing angle for the vector mesons ω and ϕ is quite small ($\approx 3.4^\circ$ [11, 12, 13]), providing an ω with nearly no $s\bar{s}$ and a ϕ being almost a pure $s\bar{s}$ state.

Therefore, instead of using the vector mesons ω and ϕ , production processes involving η' and η offer an alternative way of probing the strangeness content of the nucleon. Due to the fact that both η and η' contain a significant amount of $s\bar{s}$, but of opposite phase with respect to the nonstrange $u\bar{u} + d\bar{d}$ component, significant interference effects involving the strange-quark piece of the nu-

cleon wave function are possible [14]. In fact, it has been proposed that the relative cross sections for the reactions induced by pseudoscalar mesons, $\eta p, \eta' p \rightarrow \eta p, \eta' p, K^+ \Lambda$ and $\pi^- p \rightarrow \eta n, \eta' n$, provide a sensitive test for the presence of the $s\bar{s}$ component in the nucleon wave function [14].

Due to its nontrivial properties, the QCD vacuum exhibits strong gluonic fluctuations with pseudoscalar quantum numbers to which the $\eta_{q,s}$ states can couple via the $U_A(1)$ axial anomaly. The nonperturbative gluon dynamics and the axial anomaly [3, 4, 5, 15] are thought to be responsible for the generation of the much larger mass of η' as compared to the masses of other members of the $SU(3)$ pseudoscalar meson nonet known as the Goldstone bosons. The masses of the Goldstone bosons are generated by the spontaneous breaking of chiral symmetry [2, 6, 16]. The η' meson is, therefore, thought to couple strongly to gluons via the $U_A(1)$ axial anomaly coupling [17, 18]. The unexpectedly large branching ratio measured recently for the inclusive decay of beauty particles, $B \rightarrow \eta' + X$ [19], has been interpreted as possible experimental evidence in this respect [20]. To date, the KLOE collaboration has recently found that the gluonium content in the η' is consistent with a fraction below 15% [10]. In any case, if there is a strong coupling of η' meson to gluons, it would be conceivable that short-range reaction processes such as $pp \rightarrow pp\eta'$ might reveal the gluonic degrees of freedom in the low energy interactions involving nucleons and η' [21].

One of the properties of the η' meson of extreme importance is its yet poorly known coupling strength to the nucleon. This has attracted much attention in connection with the so-called “nucleon-spin crisis” in polarized deep inelastic lepton scattering [22]. In the zero-momentum

limit, the $NN\eta'$ coupling constant $g_{NN\eta'}$ is related to the flavor singlet axial charge G_A through the flavor singlet Goldberger-Treiman relation [23] (see also Refs.[24, 25])

$$2m_N G_A(0) = F g_{NN\eta'}(0) + \frac{F^2}{2N_F} m_{\eta'} g_{NNG}(0), \quad (2)$$

where $F \sim \sqrt{2N_F}F_\pi$ is a renormalization-group invariant decay constant; N_F and F_π denote the number of flavors and the pion decay constant, respectively. g_{NNG} describes the coupling of the nucleon to the gluons arising from contributions violating the Okubo-Zweig-Iizuka rule [26]. The EMC collaboration [22] has measured an unexpectedly small value of $G_A(0) \sim 0.20-0.35$. The first term on the right-hand side of the above equation corresponds to the quark contribution to the “spin” of the proton, and the second term to the gluon contribution [25, 27]. Therefore, if $g_{NN\eta'}(0)$ is known, Eq. (2) may be used to extract the coupling $g_{NNG}(0)$. However, unfortunately, there is no direct experimental measurement of $g_{NN\eta'}(0)$ so far. Reaction processes where the η' meson is produced directly off a nucleon, such as $\gamma p \rightarrow p\eta'$ and $pp \rightarrow pp\eta'$, may thus offer a unique opportunity to extract this coupling constant. Of course, other production mechanisms, such as meson exchange and nucleon resonance currents, must be taken into account before a quantitative determination of $g_{NN\eta'}$ is possible.

Yet another interesting aspect in studying η' production processes is that they may provide an alternative tool to extract information on nucleon resonances, N^* . Current knowledge of most of the nucleon resonances is mainly due to the study of πN scattering and/or pion photoproduction off the nucleon. Reaction processes such as η' photoproduction provide opportunities to study those resonances that couple only weakly to pions, especially, in the less explored higher N^* mass region of “missing resonances” [28]. Missing resonances are those predicted by quark models but not found in more traditional pion-production reactions [28].

In the present work, we concentrate on the reactions $\gamma p \rightarrow p\eta'$ and $pp \rightarrow pp\eta'$. So far there exists only a limited number of studies of the η' photoproduction both experimentally [29, 30] and theoretically [31, 32, 33, 34]. Zhang *et al.* [31], in their theoretical investigation using an effective Lagrangian approach, have emphasized the role of the $D_{13}(2080)$ resonance in the description of the, then, existing data [29], while Li [32] has described those data within a constituent quark model with the off-shell $S_{11}(1535)$ excitation as the dominant contribution. The authors of Ref. [30] described their data — obtained with much higher statistics than the previous measurements [29] — in the energy region from threshold to 2.6 GeV under the assumption of resonance dominance. They considered an S_{11} and a P_{11} resonance with extracted masses of 1897 and 1986 MeV, respectively. The former resonance was needed to explain the energy dependence of the total cross section which exhibits a steep rise and falloff close to threshold. The $P_{11}(1986)$ resonance was needed to account for the measured forward rising an-

gular distributions. In a calculation similar to that in Ref. [32], Zhao [34] introduced also a P_{13} and an F_{13} resonance to describe the SAPHIR data [30]. In both these quark model calculations, no (t -channel) vector meson exchange contribution was considered. Based on a $U(3)$ baryon chiral perturbation theory, Borasoy [33] introduced the off-shell $P_{11}(1440)$ and $S_{11}(1535)$ resonances, in addition to the Born and vector meson exchange contributions, to describe the data [30]. Quite recently, Chiang *et al.* [35] have put forward a model for η' photoproduction that considers the t -channel vector meson exchanges in terms of Regge trajectories to comply with high energy behavior. In their calculation, which was applied to the SAPHIR data [30] (that cover an energy region < 2.6 GeV), the interference of the Regge trajectories with an S_{11} resonance is the underlying mechanism responsible for reproducing the data and no need of any P_{11} resonance contribution was found. In contrast, also in a quite recent calculation, Sibirtsev *et al.* [36] have described the SAPHIR data by considering the t -channel ρ - and ω -meson exchange contributions with an exponential form factor at the $\gamma\eta'v$ vertex ($v = \rho, \omega$). The observed forward rise of the angular distribution is then largely accounted for by the (t -dependent) exponential form factor. In addition, the $S_{11}(1535)$ resonance is introduced in order to account for the energy dependence of the total cross section. Sibirtsev *et al.* [36] have also speculated that the η' photoproduction at high energies and large t may be useful in determining the $NN\eta'$ coupling constant $g_{NN\eta'}$. New experimental investigations of η' photoproduction are currently being carried out at JLab by the CLAS collaboration [37] and at ELSA by the Crystal Barrel collaboration [38].

The $pp \rightarrow pp\eta'$ reaction has been a subject of increasing attention in the last few years. Experimental data on total cross section exist for excess energies up to $Q \sim 24$ MeV [39], in addition to the total cross section and the angular distribution at $Q = 143.8$ MeV from the DISTO collaboration [40]. The new total cross section data in the excess energy range of $Q = 26-47$ MeV and an angular distribution at $Q = 46.6$ MeV have been just reported by the COSY-11 collaboration [41], filling in partly the gap between the near threshold [39] and higher energy DISTO data [40]. Theoretically, the $pp \rightarrow pp\eta'$ reaction has been investigated by a number of authors [42, 43] within meson-exchange approaches of varying degrees of sophistication. In particular, in Ref. [43], we have explored the possible role of the nucleonic, mesonic, and resonance current contributions. The $S_{11}(1987)$ and $P_{11}(1986)$ resonances as determined by the SAPHIR collaboration [30] have been considered for the resonance current. Due to the scarcity of the then available data (total cross sections up to $Q \approx 10$ MeV), it was not possible to quantitatively constrain each of these currents. With the increase of the data base since then, we are now in a much better position to learn about this reaction than was possible before.

The major purpose of the present work is to perform

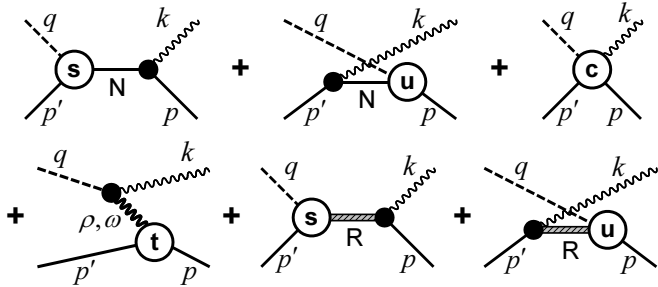


FIG. 1: Diagrams contributing to $\gamma p \rightarrow \eta' p$. Time proceeds from right to left. The intermediate baryon states are denoted N for the nucleon, and R for the S_{11} and P_{11} resonances. The intermediate mesons in the t -channel are ρ and ω . The external legs are labeled by the four-momenta of the respective particles and the labels s, u, and t of the hadronic vertices correspond to the off-shell Mandelstam variables of the respective intermediate particles. The three diagrams in the lower part of the diagram are transverse individually; the three diagrams in the upper part are made gauge-invariant by an appropriate choice (see text) of the contact current depicted in the top-right diagram. The nucleonic current (nuc) referred to in the text corresponds to the top line of diagrams; the meson-exchange current (mec) and resonance current contributions correspond, respectively, to the leftmost diagram and the two diagrams on the right of the bottom line of diagrams.

a combined analysis of the $\gamma p \rightarrow p\eta'$ and $pp \rightarrow pp\eta'$ reactions within a relativistic meson-exchange model of hadronic interactions (see Figs. 1 and 2). For the η' photoproduction, in the s and u channels, we consider contributions due to the intermediate nucleon and the nucleon resonances and in the t -channel, we take into account ρ and ω meson exchanges. Since we employ the physical coupling constants and physical masses for all intermediate particles in all the channels, the s -channel diagrams also account for the pole part of the $N\eta'$ final-state interaction (FSI) [44]. For the nonpole part of the FSI, the u and t channels correspond to the Born approximation of the corresponding $N\eta'$ T -matrix. Phenomenological form factors are attached to each vertex in all channels. The total amplitude is constrained to obey gauge invariance following the prescription of Refs. [45, 46, 47]. The photoproduction amplitude thus obtained is then used in the construction of the basic η' production amplitude in $pp \rightarrow pp\eta'$ by replacing the photons with relevant mesons which, in turn, are attached to the second nucleon (see Fig. 2). Hereafter, the basic η' production amplitude is referred to as the η' production current following the nomenclature employed in Ref. [43]. The $pp \rightarrow pp\eta'$ reaction is then described in a Distorted-Wave Born Approximation (DWBA) which includes both the nucleon-nucleon (NN) final-state interaction and the initial-state interaction (ISI).

The present paper is organized as follows. In Sec. II our model for the $\gamma p \rightarrow p\eta'$ and $pp \rightarrow pp\eta'$ reactions is described briefly. The numerical results are discussed in Sec. III, and in Sec. IV we present our summarizing

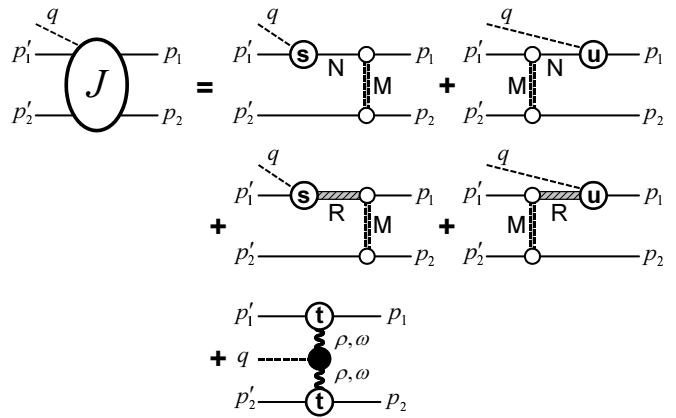


FIG. 2: Basic production mechanisms for $pp \rightarrow pp\eta'$. Time proceeds from right to left. The full amplitude, with additional initial- and final-state contributions, is given by Eq. (3). As in Fig. 1, N and R denote the intermediate nucleon and resonances, respectively, and M incorporates all exchanges of mesons π , η , ρ , ω , σ , and a_0 ($\equiv \delta$) for the nucleon graphs and π , ρ , and ω for the resonance graphs. External legs are labeled by the four-momenta of the respective particles; the hadronic vertices s, u, and t here correspond to the same kinematic situations, respectively, as those identified similarly in Fig. 1. The nucleonic, resonance, and meson-exchange contributions referred to in the text correspond, respectively, to the first, second, and third lines of the diagrams on the right-hand side.

conclusions.

II. FORMALISM

The dynamical content of our approach is summarized by the graphs of Figs. 1 and 2. For the η' photoproduction, we employ the tree graphs of Fig. 1 with form factors at the vertices to account for the hadronic structure. The gauge invariance of this production current is ensured by adding a phenomenological contact current, according to the prescription of Refs. [45, 46]. This contact term (see below) may also be thought of as mocking up the neglected parts of the final-state interaction. The hadronic $pp \rightarrow pp\eta'$ reaction is described according to the model put forward in Refs. [43, 48]. The DWBA amplitude M for this process is given by [48]

$$M = (1 + T_f G_f) J (1 + G_i T_i), \quad (3)$$

where T_n , with $n = i, f$, denotes the NN T -matrix interaction in the initial (i) or final (f) state, and G_n is the corresponding two-nucleon propagator (which absorbs the factor i found in the DWBA formula given in Ref. [48]). J sums up the basic η' production mechanisms depicted in Fig. 2. In the absence of models capable of providing a reliable off-shell NN ISI, we consider it only in the on-shell approximation following Ref. [48]. This is shown to be a reasonable approximation for calculating cross sections [49]. The NN FSI is generated by using

the Bonn potential [50]. We use the Blankenbecler-Sugar propagator for the two-nucleon propagator G_f in Eq. (3) in order to be consistent with the NN interaction used. The Coulomb force is ignored in the present calculation; its effect is known to be relevant only in the energy region very close to threshold (excess energies less than 5 MeV) [43]. In the present work we concentrate our attention on the higher excess energy region where the Coulomb effect is negligible.

The interaction Lagrangian used to construct our model for the basic production amplitudes is given below. For further convenience, we define the operators

$$\Gamma^{(+)} = \gamma_5 \quad \text{and} \quad \Gamma^{(-)} = 1. \quad (4)$$

A. Electromagnetic interaction Lagrangians

The electromagnetic vertices are derived from the following Lagrangian densities.

NN γ Lagrangian:

$$\mathcal{L}_{NN\gamma} = -e\bar{N} \left\{ \left(\gamma^\mu - \kappa_p \frac{\sigma^{\mu\nu} \partial_\nu}{2m_N} \right) A_\mu \right\} N, \quad (5)$$

where A_μ and N stand for the photon and nucleon fields, respectively. m_N is the nucleon mass, e the elementary charge unit, and $\kappa_p = 1.793$ the anomalous magnetic moment of the proton.

NN γ Lagrangian (resonance $N^ = S_{11}, P_{11}$):*

$$\mathcal{L}_{NN^*\gamma}^{(\pm)} = \frac{g_{NN^*\gamma} e}{m_{N^*} + m_N} \bar{N}^* \Gamma^{(\mp)} \sigma_{\mu\nu} (\partial^\nu A^\mu) N + \text{h. c.}, \quad (6)$$

where N^* stands for the resonance field. The upper and lower signs on the left refer to the even (+) and odd (−) parity resonances, respectively; m_{N^*} is the resonance mass and $g_{NN^*\gamma}$ the coupling constant. Both parameters are fit parameters.

$\eta'v\gamma$ Lagrangian (vector meson $v = \rho, \omega$):

$$\mathcal{L}_{\eta'v\gamma} = -\frac{g_{\eta'v\gamma} e}{m_v} \varepsilon_{\alpha\beta\nu\mu} (\partial^\alpha V^\beta) (\partial^\nu A^\mu) \eta', \quad (7)$$

where $\varepsilon^{\mu\nu\alpha\beta}$ is the Levi-Civita tensor. V^β stands for the vector meson field ($= \rho_3^\beta, \omega^\beta$). The resulting $\eta'v\gamma$ vertex is multiplied by the form factor $F_v(t)$ which describes the off-shell behavior of the intermediate vector meson with squared momentum transfer $t = (p - p')^2$ (cf. fourth diagram in Fig. 1). In general, we use the dipole form

$$F_v(t) = \left(\frac{\Lambda_v^2 - m_v^2}{\Lambda_v^2 - t} \right)^2 \quad (8)$$

(see, however, Fig. 10 below and its discussion in the text). The cutoff Λ_v , taken to be identical for both ρ and ω , is a fit parameter. The coupling constants $g_{\eta'v\gamma}$ in Eq.(7) are taken from radiative decays [12]; their signs are inferred from $SU(3)$ symmetry considerations following Ref. [43] in conjunction with the sign of the coupling constant $g_{\pi v\gamma}$ determined from a study of pion photoproduction in the 1 GeV energy region [51].

B. Hadronic interaction Lagrangians

The following Lagrangians describe the hadronic vertices.

NN η' Lagrangian:

$$\mathcal{L}_{NN\eta'} = -g_{NN\eta'} \bar{N} \left\{ \gamma_5 \left[i\lambda + \frac{1-\lambda}{2m_N} \not{\partial} \right] \eta' \right\} N, \quad (9)$$

where $\not{\partial} = \gamma_\mu \partial^\mu$.

NN η' Lagrangian (resonance $N^ = S_{11}, P_{11}$):*

$$\mathcal{L}_{NN^*\eta'}^{(\pm)} = \mp g_{NN^*\eta'} \bar{N}^* \left\{ \Gamma^{(\pm)} \left[i\lambda + \frac{1-\lambda}{m_{N^*} \pm m_N} \not{\partial} \right] \eta' \right\} N + \text{h. c.} \quad (10)$$

where the upper and lower signs on the left refer to the even (+) and odd (−) parity resonances, respectively. Following Refs. [43, 48], each of the $NB\eta'$ vertices obtained from Eqs. (9) and (10) ($B = N, N^*$) is multiplied by a phenomenological cutoff function

$$G_B(x) = \frac{\Lambda_B^4}{\Lambda_B^4 + (x - m_B^2)^2}, \quad (11)$$

which is normalized to unity, i.e., $G_B(m_B^2) = 1$. The variable x is the squared four-momentum of the intermediate off-shell baryon B , whose mass m_B is equal to either the nucleon mass m_N or the mass of the resonance, m_{N^*} . The cutoff $\Lambda_B = 1200$ MeV is taken as the same for all baryons. The parameters $\lambda \equiv \lambda_{NB\eta'}$ in Eqs. (9) and (10) describing the mixing of pseudoscalar and pseudovector contributions and the coupling constants $g_{NB\eta'}$ are individual fit parameters for each of the three baryon states considered here. (As the subsequent discussion shows, the fits prefer couplings that are almost entirely pseudovector for the nucleon, i.e., $\lambda_{NN\eta'} \approx 0$, and almost entirely pseudoscalar for the resonances, i.e., $\lambda_{NN^*\eta'} \approx 1$.)

vv η' Lagrangian (vector meson $v = \rho, \omega$):

$$\mathcal{L}_{\rho\rho\eta'} = -\frac{g_{\rho\rho\eta'}}{2m_\rho} \varepsilon_{\alpha\beta\nu\mu} (\partial^\alpha \vec{\rho}^\beta) \cdot (\partial^\nu \vec{\rho}^\mu) \eta', \quad (12a)$$

$$\mathcal{L}_{\omega\omega\eta'} = -\frac{g_{\omega\omega\eta'}}{2m_\omega} \varepsilon_{\alpha\beta\nu\mu} (\partial^\alpha \omega^\beta) (\partial^\nu \omega^\mu) \eta', \quad (12b)$$

where $\vec{\rho}^\mu$ and ω^β stand for the ρ and ω meson fields, respectively. Each of the resulting $vv\eta'$ vertices is multiplied by a product of form factors, $\tilde{F}_v(q_1^2) F_v(q_2^2)$, where $q_1 = p_1 - p'_1$ and $q_2 = p_2 - p'_2$ (cf. last diagram in Fig. 2). The form factor

$$\tilde{F}_v(q^2) = \left(\frac{\Lambda_v^2}{\Lambda_v^2 - q^2} \right)^2 \quad (13)$$

associated with one of the intermediate off-shell vector mesons is the same as in Eq. (8), with the same cutoff masses Λ_v , except for the normalization point, consistent with the kinematics at which the coupling constants $g_{vv\eta'}$ are extracted. The $g_{vv\eta'}$ are obtained from a systematic

analysis of the radiative decay of vector and pseudoscalar mesons based on $SU(3)$ symmetry considerations in conjunction with vector-meson dominance arguments [43]. Hence, there are no free *independent* parameters for this vertex.

$NN^*\pi$ Lagrangian (resonance $N^* = S_{11}, P_{11}$):

$$\mathcal{L}_{NN^*\pi}^{(\pm)} = \mp \frac{g_{NN^*\pi}}{m_{N^*} \pm m_N} \bar{N}^* \Gamma^{(\pm)} (\not{\partial} \vec{\pi}) \cdot \vec{\tau} N + \text{h.c.}, \quad (14)$$

where $\vec{\pi}$ denotes the pion field. Again, each of the resulting $NN^*\pi$ vertices is multiplied by a product of form factors, $G_{N^*}(x)G_\pi(q_\pi^2)$; q_π is the pion's four-momentum and x , as before, is the squared four-momentum of the intermediate N^* state. The form factor G_{N^*} here is exactly the same as in Eq. (11) for $B = N^*$, with $\Lambda_{N^*} = 1200 \text{ MeV}$. G_π is the pion form factor parametrization from the Bonn potential, with a cutoff-mass value of 900 MeV. For this vertex, therefore, the coupling constant $g_{NN^*\pi}$ is the only additional fit parameter.

NN^*v Lagrangian (vector meson $v = \rho, \omega$; resonance $N^* = S_{11}, P_{11}$):

$$\mathcal{L}_{NN^*v}^{(\pm)} = \frac{g_{NN^*v}}{m_{N^*} + m_N} \bar{N}^* \Gamma^{(\mp)} \sigma_{\mu\nu} (\partial^\nu V^\mu) N + \text{h.c.}, \quad (15)$$

where $V^\mu = \vec{\rho}^\mu \cdot \vec{\tau}$, ω^μ . Each resulting vertex is multiplied by a product of form factors, $G_{N^*}(x)F_v(q_v^2)$; q_v is the vector meson's four-momentum and x has the same meaning as before. The parameters of G_{N^*} and F_v are fixed already; the coupling constant g_{NN^*v} , therefore, is the only fit parameter here.

All of the remaining MNN vertices (meson $M = \pi, \eta, \rho, \omega, \sigma, a_0$) are parametrized as in the Bonn potential [50]. The only exceptions are the values of the coupling constant $g_{NN\omega} = 10$, the pseudoscalar-pseudovector (ps-pv) mixing parameter $\lambda_{NN\pi} = 0$, and the cutoff-mass value of 900 MeV at the $NN\pi$ vertex used in the resonance and meson exchange currents (see discussion in Refs. [48, 52]).

Throughout this work, the widths of the nucleon resonances are fixed to be $\Gamma_{N^*} = 150 \text{ MeV}$ ($N^* = S_{11}, P_{11}$). We neglect their energy dependence in order to keep the analysis simple. Certainly, such a feature should be taken into account when aiming at a more quantitative extraction of the resonance parameters with data more accurate than what are available at present.

In the present work we restrict ourselves to contributions from π, ρ , and ω meson exchanges in the resonance currents in describing the $pp \rightarrow pp\eta'$ reaction. Also, in contrast to Ref. [43], we omit the $\sigma\eta\eta'$ -exchange current in the present work because it is much less under control than the dominant $vv\eta'$ -exchange contribution and its inclusion would introduce additional uncertainties in the model.

C. Gauge-invariance preserving contact term

Employing form factors for the s - and u -channel contributions to the photoproduction amplitude containing

an intermediate nucleon (see the first two diagrams in Fig. 1) and allowing for pseudovector couplings in the $NN\eta'$ vertex in general destroys the gauge invariance of the production amplitude. Within the present context of a model approach, to restore gauge invariance requires the introduction of phenomenological contact-type currents.

Following here the prescription given in Refs. [45, 46], there are two basic contributions necessary to ensure gauge invariance for the present application to $\gamma p \rightarrow p\eta'$. The first contribution,

$$j_{\text{KR}}^\mu = -e g_{NN\eta'} (1 - \lambda_{NN\eta'}) \frac{\gamma_5 \gamma^\mu}{2m_N} [G_N(s) - G_N(u)], \quad (16)$$

corresponding to the Kroll-Ruderman current of pion photoproduction, cancels the gauge-invariance-violating terms arising from using pseudovector couplings. The form factors G_N here correspond to Eq. (11). The second gauge-invariance preserving (GIP) contribution,

$$j_{\text{GIP}}^\mu = -e g_{NN\eta'} \gamma_5 \frac{(2p+k)^\mu}{s - m_N^2} [G_N(s) - \hat{F}] - e g_{NN\eta'} \gamma_5 \frac{(2p'-k)^\mu}{u - m_N^2} [G_N(u) - \hat{F}], \quad (17)$$

is necessary because our model employs form factors at the vertices. As far as gauge invariance is concerned, the function \hat{F} here is arbitrary. Analyticity, on the other hand, requires that this current be free of singularities, i.e., it must be a *contact* current. One of the simplest choices for \hat{F} in the present context then is¹

$$\hat{F} = 1 - [G_N(s) - 1][G_N(u) - 1]. \quad (18)$$

This corresponds to the choice advocated in Ref. [47] on the grounds of crossing symmetry. The resulting GIP current then is

$$j_{\text{GIP}}^\mu = -e g_{NN\eta'} \gamma_5 (2p+k)^\mu G_N(u) \frac{G_N(s) - 1}{s - m_N^2} - e g_{NN\eta'} \gamma_5 (2p'-k)^\mu G_N(s) \frac{G_N(u) - 1}{u - m_N^2}, \quad (19)$$

which evidently is free of any singularities. Adding the sum of the Kroll-Ruderman term (16) and the GIP current (19) restores gauge invariance for the present model; in Fig. 1, they correspond to the rightmost diagram in the top row of diagrams.

¹ In Refs. [45, 46], it was argued that, for simplicity, one should choose to describe \hat{F} in terms of the existing form factors of the problem at hand. The most general ansatz then would be

$$\hat{F}(s, u, t) = 1 - \sum_{i,j,k} \alpha_{ijk} [G_s(s)]^i [G_u(u)]^j [G_t(t)]^k,$$

where G_s, G_u , and G_t are the s -, u -, and t -channel form factors. The simplest choice that is free of singularities is then given by restricting the sum to $i, j, k = 0, 1$ and putting $\alpha_{ijk} = (-1)^{i+j+k}$. Equation (18) follows with $G_t \equiv 0$ and $G_s = G_u = G_N$.

TABLE I: Model parameters fitted to the $\gamma p \rightarrow \eta' p$ and $pp \rightarrow pp\eta'$ data. The dipole form factor is used at the electromagnetic vertex in the mesonic current [cf. Eq. (8)]. Below, “Bonn” indicates that the same values as in the Bonn NN potential B (Table A.1) [50] are used. (†) indicates that the values of $g_{NN\omega} = 10$ and $(\lambda_{NN\pi}, \Lambda_{NN\pi}) = (0, 900 \text{ MeV})$ overwrite those of the Bonn potential. The widths of the resonances $N^* = S_{11}, P_{11}$ are fixed to be $\Gamma_{N^*} = 150 \text{ MeV}$. Also, the pseudovector coupling ($\lambda = 0$) is used at the $NN^*\pi$ vertices. Values in boldface are not fitted. Column (a) includes only the meson-exchange current (mec) and the S_{11} resonance current. Adding either the nucleonic (nuc) or a P_{11} resonance current contribution produces the results of columns (b) and (c), respectively. In (d), successively stronger (as indicated by the values of the $g_{NN\eta'}$ coupling constant in square brackets) nucleonic contributions are added to the mec + S_{11} + P_{11} contribution.

Coupling constant	(a)	(b)	(c)	(d)
Nucleonic current:				
$(g_{NN\gamma}, \kappa_p)$		(e, 1.793)		(e, 1.793)
$(g_{NN\eta'}, \lambda)$		(2.22, 0.05)		([1, 2, 3], 0)
Λ_N (MeV)		1200		1200
MNN [$M = \pi, \eta, \rho, \omega, \sigma, a_0$]		Bonn		Bonn
Mesonic current:				
$g_{\eta'\rho\gamma}$	1.25	1.25	1.25	1.25
$g_{\eta'\omega\gamma}$	0.44	0.44	0.44	0.44
Λ_v (MeV)	1383	1253	1400	[1286, 1257, 1225]
$g_{\eta'\rho\rho}$	4.94	4.94	4.94	4.94
$g_{\eta'\omega\omega}$	4.90	4.90	4.90	4.90
MNN [$M = \rho, \omega$](†)	Bonn	Bonn	Bonn	Bonn
$N^* = S_{11}$ current:				
m_{N^*} (MeV)	1760	1536	1646	[1650, 1650, 1650]
$(g_{NN^*\gamma} g_{NN^*\eta'}, \lambda)$	(0.68, 1.00)	(4.16, 1.00)	(3.56, 0.76)	[(2.22, 0.98), (2.45, 1.00), (2.61, 1.00)]
Λ_{N^*} (MeV)	1200	1200	1200	1200
$g_{NN^*\pi} g_{NN^*\eta'}$	3.62	16.34	11.11	[2.62, 4.37, 4.77]
$g_{NN^*\rho} g_{NN^*\eta'}$	-0.49	-2.25	11.25	[11.01, 7.23, 6.69]
$g_{NN^*\omega} g_{NN^*\eta'}$	0.24	7.75	-1.93	[-14.44, -5.16, -2.04]
MNN [$M = \pi, \rho, \omega$](†)	Bonn	Bonn	Bonn	Bonn
$N^* = P_{11}$ current:				
m_{N^*} (MeV)			1873	[1870, 1849, 1852]
$(g_{NN^*\gamma} g_{NN^*\eta'}, \lambda)$			(4.60, 0.82)	[(3.28, 0.97), (1.88, 0.90), (0.27, 0.97)]
Λ_N (MeV)			1200	1200
$g_{NN^*\pi} g_{NN^*\eta'}$			6.04	[4.61, 6.98, 9.45]
$g_{NN^*\rho} g_{NN^*\eta'}$			-2.20	[-6.05, -4.99, -4.71]
$g_{NN^*\omega} g_{NN^*\eta'}$			-20.53	[-28.69, -32.24, -28.35]
MNN [$M = \pi, \rho, \omega$](†)			Bonn	Bonn

III. RESULTS AND DISCUSSION

The basic strategy of our model approach is to first fix the free parameters of the photoproduction reaction and then go to the hadronic process to fix the remaining parameters.

The results for coupling constants and resonance masses, etc., given here were obtained by standard best-fit procedures. At present, however, the quality of the data is not good enough to provide really stringent constraints for the fits. As discussed also in detail below, in many instances, therefore, the parameters obtained here may be changed within certain limits without affecting the overall quality of the fits. In this situation, χ^2 values

for the fits carry little information and were omitted from the tables.

The steep rise and fall of the measured total cross section in $\gamma p \rightarrow p\eta'$ close to threshold [29, 30] suggests the presence of an S_{11} nucleon resonance contribution. Of course, one should always keep in mind that there is also the possibility of a threshold cusp effect, as discussed in Ref. [53], that might explain the observed behavior of the photoproduction total cross section close to threshold in the absence of any resonance. This requires further careful considerations. Here we assume the observed behavior of the cross section to be due to the nucleon resonance. Therefore, we first consider the $N^* = S_{11}$ resonance current. The mass of the resonance as well

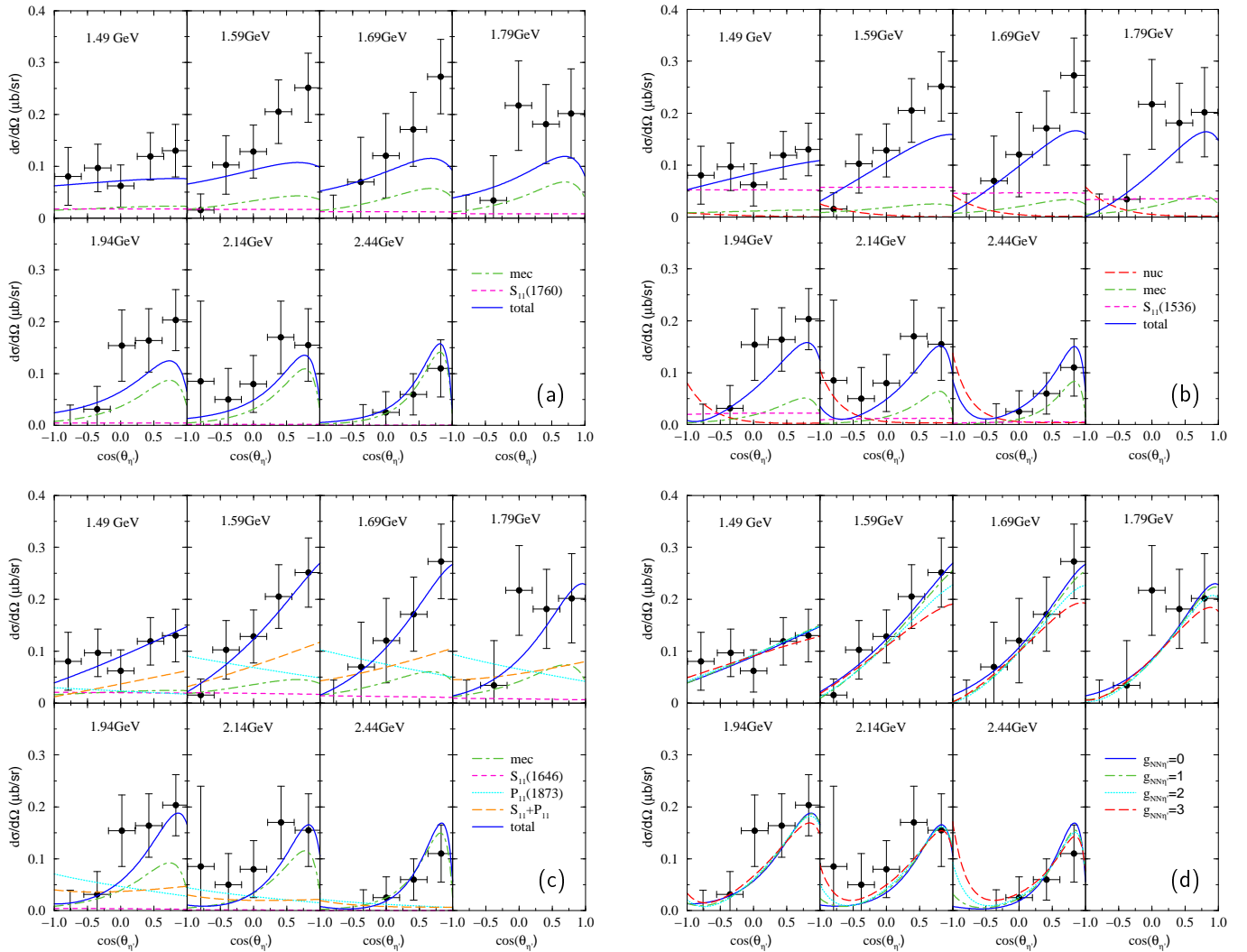


FIG. 3: (Color online) Differential cross section for $\gamma p \rightarrow p\eta'$ according to the mechanisms shown in Fig. 1. Panel (a) includes only the meson-exchange current (mec) and the S_{11} resonance. Adding either the nucleonic (nuc) contribution or a P_{11} resonance produces the results of panels (b) and (c), respectively. In (d), successively stronger (as indicated by the values of the $g_{NN\eta'}$ coupling constant) nucleonic contributions are added to the results shown in panel (c). In each case, the model parameters are determined by best fits. The meaning of the corresponding lines is indicated in the panels. The data are from Ref. [30].

as the product of the coupling constants, $g_{NN^*\gamma}g_{NN^*\eta'}$, and the ps-pv mixing parameter at the $NN^*\eta'$ vertex are free parameters to be fitted to the measured angular distributions from 1.49 to 2.44 GeV [30]. In addition to the S_{11} resonance, we also consider the ρ and ω meson-exchange currents in the t -channel. For this current, the coupling constants at the production vertices $\eta'v\gamma$ ($v = \rho, \omega$) are known from the radiative decay of η' , $\eta' \rightarrow v + \gamma$. Also, since the relevant hadronic vertices NNv are known from other studies, the only unknown parameter in the mesonic current is the cutoff parameter Λ_v in the form factor at the $\eta'v\gamma$ vertex [cf. Eq. (7)]. Together with the free parameters of the S_{11} resonance, it has also been fitted to the data. The resulting parameter values are quoted in Table I(a), and the corresponding angular distributions in Fig. 3(a). Here, the mass of the

S_{11} resonance results to be $m_{S_{11}} = 1760$ MeV; however, inclusion of other currents into the fitting procedure will change its value as we shall show below. As one can see from the figure, the $S_{11}(1760)$ current contribution decreases as the energy increases while the mesonic current contribution increases with the energy and rises at forward angles. At lower energies, the constructive interference between the two currents is important in enhancing the cross section, although it is not sufficient to reproduce the forward rise exhibited by the data. At higher energies, the mesonic current dominates almost completely and describes nicely the observed angular distribution. Therefore, the mesonic current is fixed to a large extent by the forward angle data at higher energies.

Fig. 3(b) shows the results when the nucleonic current is added to the S_{11} resonance and mesonic currents.

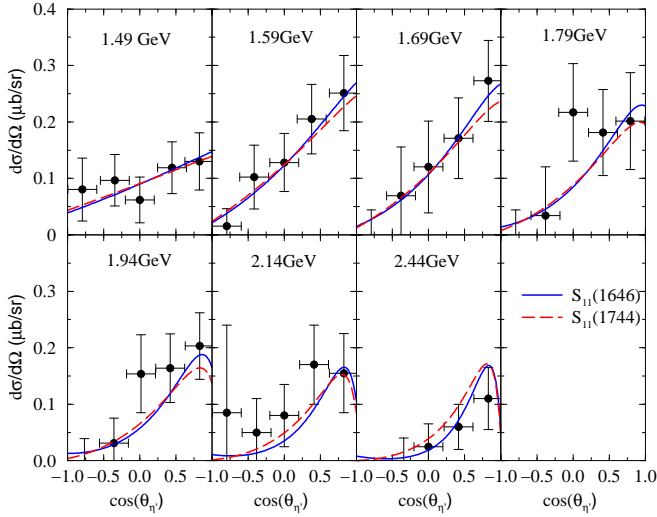


FIG. 4: (Color online) Two fits resulting in different sets of the extracted resonance mass values. Both fits include the S_{11} and P_{11} resonances as well as the meson-exchange currents. The solid curves are the same ones shown in Fig. 3(c) with the mass values of $(m_{S_{11}}, m_{P_{11}}) = (1646, 1873)$ MeV. For the dashed curves, the corresponding mass values are $(1744, 1879)$ MeV.

In the nucleonic current, both the $NN\eta'$ coupling constant $g_{NN\eta'}$ and the corresponding ps-pv mixing parameter $\lambda_{NN\eta'}$ are fitted to the data. The parameters in the mesonic and S_{11} resonance currents are refitted to the data altogether. The corresponding values are given in Table I(b). The nucleonic current contribution (long-dashed curves) is small at lower energies but increases with energy at backward angles due to the u -channel diagram, a feature that has been also realized in Ref. [36]. Therefore, measurements at high energy and backward angles (large t) will help constrain the poorly known $NN\eta'$ coupling constant $g_{NN\eta'}$. We will come back to further discussion of this issue later. The S_{11} resonance contribution (dashed curves) is larger than that shown in Fig. 3(a) at lower energies which improves the description of the data in this energy region. It also exhibits a stronger energy dependence. The fitted value of the resonance mass is now $m_{S_{11}} = 1536$ MeV. A comparison with the value of $m_{S_{11}} = 1760$ MeV obtained in Fig. 3(a) illustrates how this parameter value changes with the inclusion of different production mechanisms. Due to a constructive interference between the nucleonic plus resonance current and the mesonic current in the forward angle region at higher energies, the latter contribution is somewhat smaller than in Fig. 3(a). The overall description of the data is improved with respect to that in Fig. 3(a).

Fig. 3(c) illustrates the effect of the P_{11} resonance in $\gamma p \rightarrow p\eta'$. The mass of the P_{11} resonance as well as the product of the coupling constants, $g_{NN^*\gamma}g_{NN^*\eta'}$, and the ps-pv mixing parameter at the $NN^*\eta'$ vertex ($N^* = P_{11}$) are free parameters to be fitted to the data together with

the parameters in the other currents. The resulting parameter values are given in Table I(c). Here, the nucleonic current has been switched off [it will be considered in the results shown in Fig. 3(d)]. As can be seen, the P_{11} resonance contribution (dotted curves) rises at backward angles; it also rises and falls with energy. The S_{11} resonance contribution (dashed curves) is relatively small, but its interference with the P_{11} resonance contribution results in a total resonance current contribution (long-dashed curves) that rises at forward angles. Again, the mesonic current (dash-dotted curves) dominates at higher energies. The solid curves correspond to the total contribution. The overall agreement with the data is excellent, showing that the P_{11} resonance may be required for a quantitative description of the data. For a more definite conclusion about the role of the P_{11} resonance more accurate data are called for. The fitted masses of the S_{11} and P_{11} resonances are $m_{S_{11}} = 1646$ MeV and $m_{P_{11}} = 1873$ MeV, respectively. Since an excellent agreement with the data is achieved at this point, we might identify the S_{11} resonance with the known $S_{11}(1650)$ resonance [12], whose quoted width is $\Gamma_{S_{11}} = 180$ MeV. (Recall that, in this work, we have used a constant width of $\Gamma_{N^*} = 150$ MeV for all the resonances.) The P_{11} resonance does not correspond to any known resonance; it is tempting to identify it with one of the missing resonances with $m_{P_{11}} = 1880$ MeV and with the corresponding width of $\Gamma_{P_{11}} = 155$ MeV, predicted by quark models [28, 54]. Recently, an evidence for this resonance has been found in a three-channel unitary model analysis [55]. However, we emphasize that such an identification from the present analysis is premature as we shall show later in connection with the results in Fig. 4.

The role of the nucleonic current is illustrated in Fig. 3(d). Here, each curve corresponds to a given value of the $NN\eta'$ coupling constant $g_{NN\eta'}$ as indicated. The pseudovector coupling ($\lambda_{NN\eta'} = 0$) is adopted. We mention that we have also considered the pseudoscalar coupling ($\lambda_{NN\eta'} = 1$), but the fits do not support this choice and prefer to have a small value of $\lambda_{NN\eta'}$ close to zero.² For each value of $g_{NN\eta'}$, the parameters of the resonance and mesonic currents have been refitted to best reproduce the data; the values are given in Table I(d). Here, the mass of the S_{11} resonance is fixed at 1650 MeV. The solid curves corresponding to the choice $g_{NN\eta'} = 0$ are the same results as shown in Fig. 3(c). As one can see again, the major effect of the nucleonic current shows up at higher energies and backward angles in the pho-

² If we choose pure pseudoscalar coupling ($\lambda_{NN\eta'} = 1$), we find that there is a strong transition between the positive and negative energy components of the nucleon wave functions in the final and intermediate states, respectively, since the intermediate nucleon is far off-shell owing to the fact that the present reaction involves the production of a massive particle (η'). As a result, the nucleonic current contribution becomes large for this choice of the coupling and this is not supported by the data.

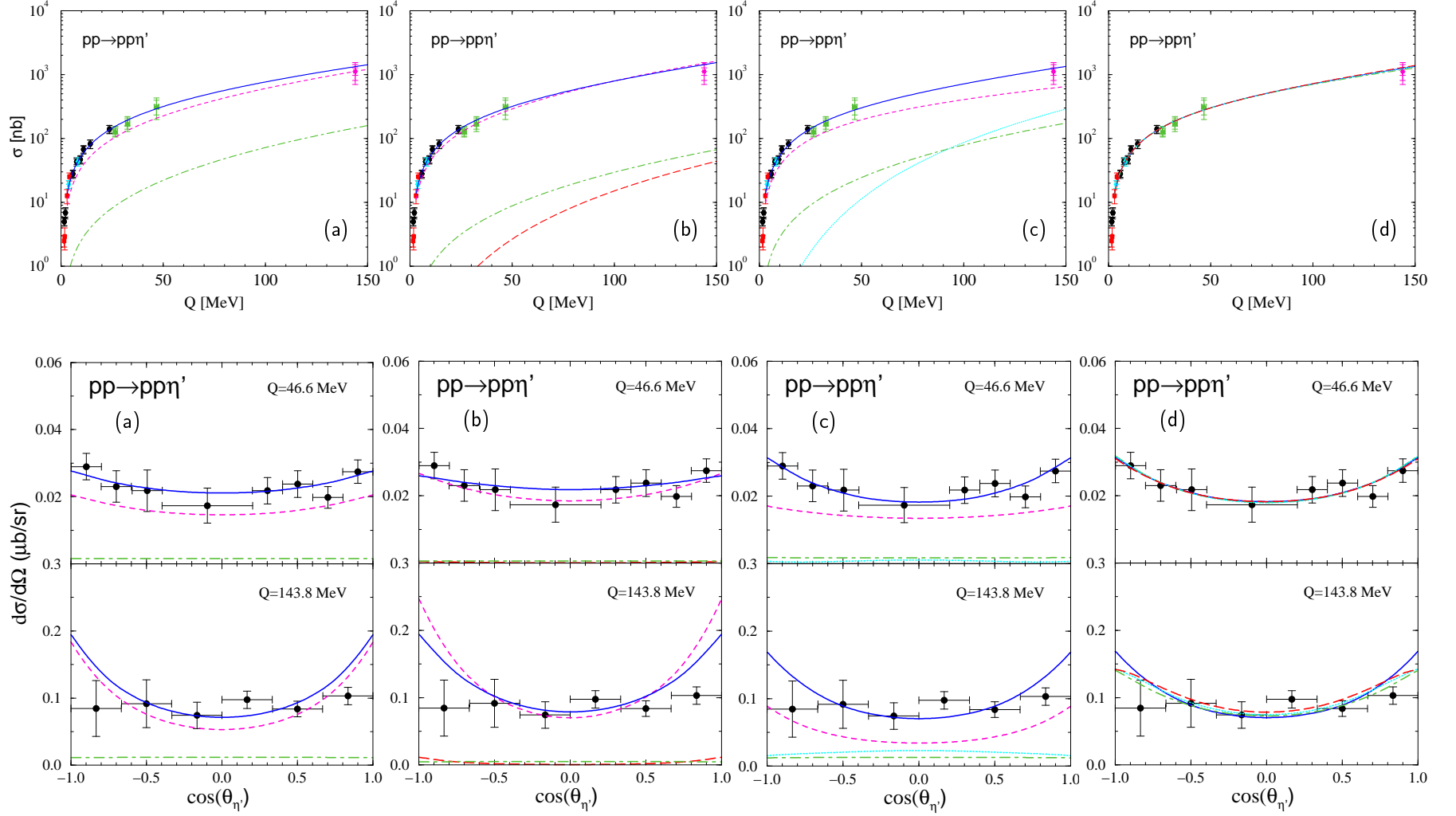


FIG. 5: (Color online) Excess energy, Q , dependence of the total cross section (top row of diagrams) and angular distributions at $Q = 46.6$ and 143.8 MeV in the c.m. frame of the system (bottom row) for $pp \rightarrow pp\eta'$, according to the mechanisms depicted in Fig. 2. The panels labeled (a)–(d) in both rows correspond to the respective panels (a)–(d) in Fig. 3, and all line styles are explained there. In part (d) of the total cross section and in the corresponding 47-MeV angular distribution, on the present scales, all curves practically lie on top of each other, i.e., these results are very insensitive to the nucleonic contributions. The total cross sections comprise data from Refs. [39, 40, 41]; the angular distribution data are from the COSY-11 collaboration (47 MeV) [41] and from DISTO (144 MeV) [40]. The calculations shown here incorporate *all three* data sets in the determination of the hadronic resonance coupling parameters (in contrast to the results shown in Fig. 7 below).

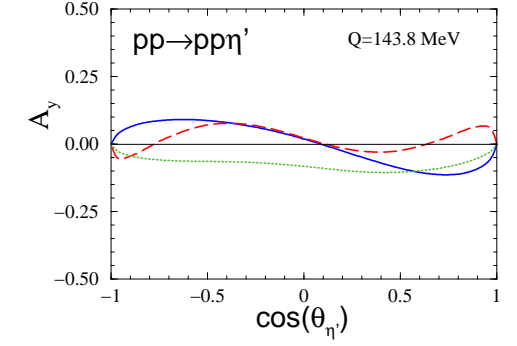
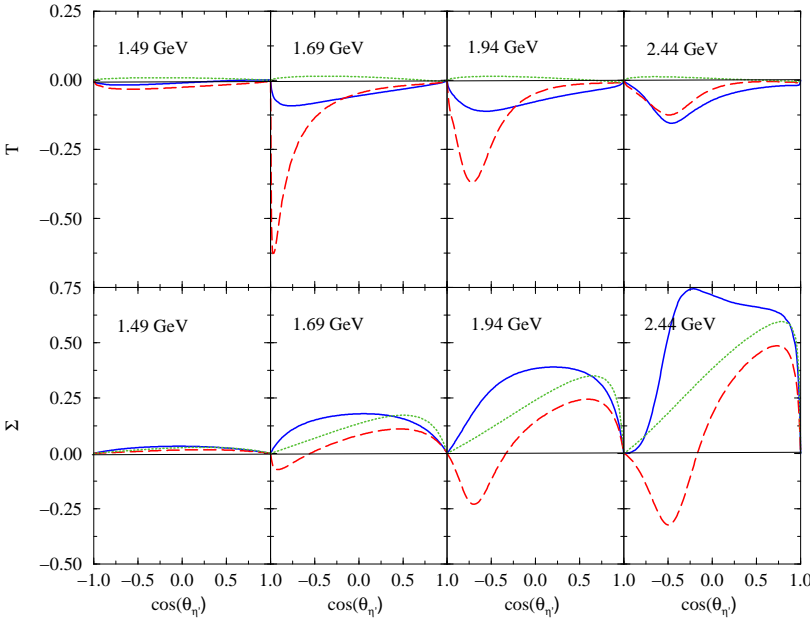


FIG. 6: (Color online) Target and photon asymmetries T and Σ , respectively, for $\gamma p \rightarrow p\eta'$ and analyzing power A_y for $pp \rightarrow pp\eta'$. The solid lines correspond to the parameters for the (d) panels in Figs. 3–5, with $g_{NN\eta'} = 0$. The dashed lines are obtained when $g_{NN\eta'} = 3$. The dotted lines correspond to the parameters for the (a) panels in Figs. 3–5, where both the P_{11} and nucleonic currents are absent.

toproduction reaction. Accurate measurements in these kinematic regions are called for. In any case, judging from the overall results, the existing data do not support values much larger than $g_{NN\eta'} = 3$. In fact, they seem to prefer smaller value of $g_{NN\eta'}$, compatible with 0. This is considerably smaller than the value of $g_{NN\eta'} = 6.1$ used in our previous work [43] on $pp \rightarrow pp\eta'$, and it is more in line with estimates based on the dispersion method [56].

As discussed in the Introduction, such a small value of the $NN\eta'$ coupling would have an important implication in connection to the “spin puzzle” of the nucleon. A recent estimate [7] of $g_{NN\eta'}$ based on an alternative formula to Eq. (2) (neglecting the higher excited pseudoscalar states or glueballs which are assumed to be negligible) in conjunction with the measured value of the singlet axial charge yields a value of $g_{NN\eta'}(0) = 1.4 \pm 1.1$. It should be noted that the $NN\eta'$ coupling constant entering in Eq. (2) is at zero momentum squared, $g_{NN\eta'}(q^2 = 0)$, while the coupling constant $g_{NN\eta'}$ in the present work is defined at the on-shell momentum squared, $q^2 = m_{\eta'}^2$. We emphasize that the relatively small value of $g_{NN\eta'}$ found here is a model-dependent result. In particular, what is relevant in our model is the product of the $NN\eta'$ coupling constant and the corresponding off-shell form factor. Since the intermediate nucleon in the nucleonic current is far off-shell due to the large mass of the produced η' meson, the result is sensitive to the choice of the form factor. As mentioned in the preceding section, the form factor used at the $NN\eta'$ vertex is the same as that used consistently in our investigation of other meson production processes.

In Fig. 4 we show a comparison of two fit results for $\gamma p \rightarrow p\eta'$, in which both the S_{11} and P_{11} resonance currents were considered in addition to the meson exchange current. The solid curves are the same results shown in Fig. 3(c) with the resulting resonance masses

of $m_{S_{11}} = 1646$ MeV and $m_{P_{11}} = 1873$ MeV. The dashed curves correspond to a fit with the resulting resonance masses of $m_{S_{11}} = 1744$ MeV and $m_{P_{11}} = 1879$ MeV. For this fit, the values of the remaining fit parameters are very close to the corresponding values quoted in Table I(c), except for the value of $g_{NN^*\gamma}g_{NN^*\eta'} = 2.07$ for $N^* = S_{11}$ which compensates for the change in the value of $m_{S_{11}}$. As one can see, the quality of the fit is essentially the same in both cases; yet, the extracted values of $m_{S_{11}}$ differ by ~ 100 MeV from each other. (See also the results of a Regge trajectory calculation in Fig. 9, where the mass of the P_{11} resonance varies substantially.) This illustrates the order of uncertainties involved in the identification of the resonances from the differential cross section data only (at least from those currently available and from the type of analysis employed here). For a more definitive identification of the resonances, one probably needs more exclusive data than the cross sections, such as the spin observables shown in Fig. 6, which can impose more stringent constraints. A further investigation of this issue is certainly required.

The results for the $pp \rightarrow pp\eta'$ reaction are shown in Fig. 5. The two panels labeled (a) include the $S_{11}(1760)$ resonance and the mesonic currents; they correspond to the photoproduction results of Fig. 3(a). All the relevant parameters for the latter reaction are taken over unchanged. Thus, the additional parameters to be fitted for the hadronic reaction concern the three products of the coupling constants, $g_{NN^*\pi}g_{NN^*\eta'}$, $g_{NN^*\rho}g_{NN^*\eta'}$, and $g_{NN^*\omega}g_{NN^*\eta'}$ [where $N^* = S_{11}(1760)$], corresponding to the three mesons exchanged between the two interacting nucleons in the resonance current (see Fig. 2). The resulting values are given in Table I(a). As can be seen here, the dominant contribution is the $S_{11}(1760)$ resonance current (dashed curves). The mesonic current is relatively small. The total cross section is nicely

reproduced, as well as the measured angular distribution at $Q = 47$ MeV.³ The latter exhibits some angular dependence although it might be compatible with a flat shape within the given experimental uncertainties. The completely flat angular distribution measured at $Q = 144$ MeV, however, is not reproduced. As one can see, the calculated angular dependence is introduced by the S_{11} resonance and it arises due to the recoil of this resonance in the overall center-of-mass (c.m.) frame.

Fig. 5(b) shows the results for $pp \rightarrow pp\eta'$ which include the nucleonic, $S_{11}(1536)$ resonance, and mesonic currents. Some of the parameters are fixed from the photoproduction reaction corresponding to Fig. 3(b). As before, the remaining parameters are fitted to the $pp \rightarrow pp\eta'$ data and are given in Table I(b). Here, for the purpose of consistency, one could, in principle, employ the coupling constants at the MNN^* vertex ($M = \pi, \eta, \rho, \omega$) for $N^* = S_{11}(1535)$ resonance as determined from our recent study of the $pp \rightarrow pp\eta$ reaction [57]. We would then have the coupling constant $g_{NN^*\eta'}$ as the only free parameter to be fitted. However, we have opted not to do so because Ref. [57] did not aim for a quantitative determination of those coupling constants. As can be seen here, the $S_{11}(1536)$ resonance current (dashed curves) gives nearly the whole contribution to the cross sections. The mesonic current is small followed by the nucleonic current. This is in contrast to the results in our previous work [43], where due to the scarcity of the then available data, it had not been possible to constrain the individual current contributions. The solid curves correspond to the total contribution. They exhibit similar features to those shown in Fig. 5(a). Here, the model tends to overestimate the total cross section at high energies although it still lies within the experimental uncertainties. We may conclude, therefore, that the addition of the nucleonic current at this stage does not improve the agreement with the data.

Next, we add the $P_{11}(1873)$ resonance to the mesonic and $S_{11}(1646)$ resonance contributions. The results are shown in Fig. 5(c). Again, all parameters relevant for the corresponding photoproduction reaction results of Fig. 3(c) are taken over. The additional parameters fitted for the hadronic reaction are given in Table I(c). It is interesting to note that, unlike in the photoproduction, here the $P_{11}(1873)$ contribution is much smaller than that from $S_{11}(1646)$. The latter is the dominant current. The angular distribution at $Q = 144$ MeV is somewhat improved; however, still in disagreement with the data. This issue is further discussed in Fig. 7.

Fig. 5(d) illustrates the influence of the nucleonic current in the $pp \rightarrow pp\eta'$ reaction. The corresponding fitted parameters are given in Table I(d). As one can see, this

reaction is rather insensitive to the nucleonic current contribution. This corroborates the statement in our earlier work [43].

Fig. 6 illustrates the sensitivity of some of the spin observables to the coupling constant $g_{NN\eta'}$ and also to the P_{11} resonance. In the left panel the target (T) and photon (Σ) asymmetries in the $\gamma p \rightarrow p\eta'$ reaction are shown. As can be seen, the target asymmetry is sensitive to $g_{NN\eta'}$ at backward angles around 1.69–1.94 GeV (compare the solid and dashed curves). However, this is the region where the cross section is very small. The photon asymmetry becomes sensitive at higher energies and in a wider range of the η' emission angle. This observable, therefore, may be helpful in constraining $g_{NN\eta'}$ more than just simple cross sections. The sensitivity to the P_{11} resonance can be assessed by comparing the dotted (without P_{11}) and solid (with P_{11}) curves. It is interesting to note that the influence of this resonance has a different pattern than that of the nucleonic current. The right panel shows the sensitivity of the analyzing power in the $pp \rightarrow pp\eta'$ reaction. Although the cross sections are rather insensitive to both $g_{NN\eta'}$ and P_{11} resonance, this observable exhibits some degree of sensitivity.

In order to investigate the discrepancy between our model results and the measured flat angular distribution at $Q = 144$ MeV for $pp \rightarrow pp\eta'$, we have repeated the calculation shown in Fig. 5 excluding the COSY-11 angular distribution data at $Q = 47$ MeV from fitting. The resulting values of the hadronic couplings are displayed in Table II and the corresponding cross sections in Fig. 7. Although the total cross sections are reproduced with the same quality as in Fig. 5, the angular distributions shown in panels (a)–(d) at $Q = 144$ MeV are now much flatter and bring the model results in better agreement with the data at this energy. Here, the less pronounced angular distribution is due to a flatter S_{11} resonance contribution which, in turn, is due to the change in the excitation mechanism of this resonance, in particular, due to interference effects among the exchanged meson (π, ρ, ω) contributions in the S_{11} resonance cur-

TABLE II: Same as in Table I, except that here the angular distribution data at $Q = 46.6$ MeV in $pp \rightarrow pp\eta'$ were excluded from fitting. Only those parameters affected by this exclusion in the fitting procedure are displayed.

coupling constant	(a)	(b)	(c)	(d)
$N^* = S_{11}$ current:				
$g_{NN^*\pi}g_{NN^*\eta'}$	-0.03	13.33	10.02	[0.05,0.98,3.28]
$g_{NN^*\rho}g_{NN^*\eta'}$	5.49	4.48	9.23	[14.53,11.92,8.42]
$g_{NN^*\omega}g_{NN^*\eta'}$	1.27	2.30	7.41	[2.25,6.31,4.25]
$N^* = P_{11}$ current:				
$g_{NN^*\pi}g_{NN^*\eta'}$			3.92	[13.01,1.54,16.47]
$g_{NN^*\rho}g_{NN^*\eta'}$			-7.83	[10.21,-3.90,8.81]
$g_{NN^*\omega}g_{NN^*\eta'}$			20.70	[5.17,12.23,18.16]

³ The excess energy Q is defined as $Q \equiv \sqrt{s} - \sqrt{s_0}$, where \sqrt{s} denotes the total energy of the system and $\sqrt{s_0} = 2m_N + m_{\eta'}$ its η' -production threshold energy.

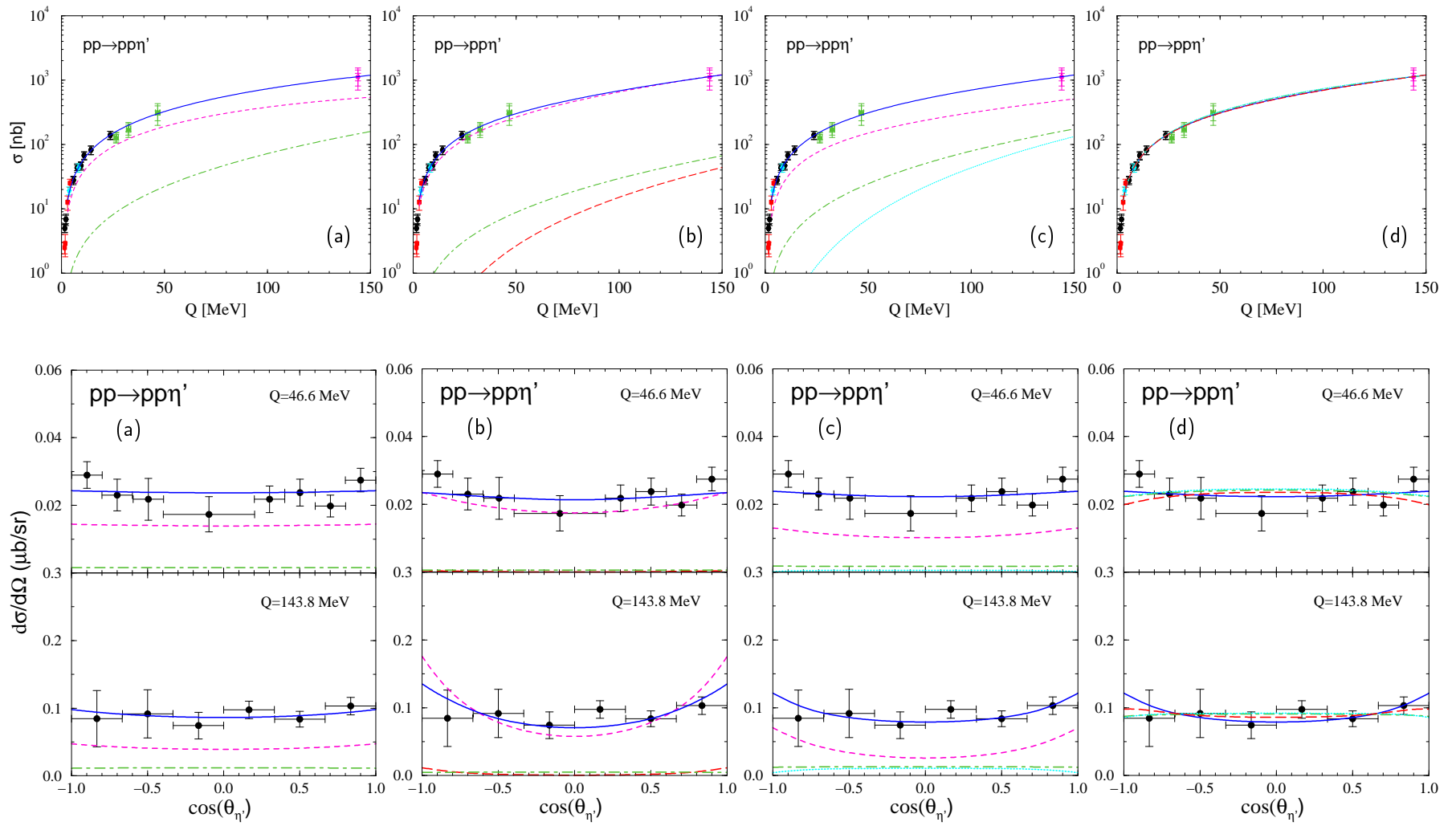


FIG. 7: (Color online) Same as Fig. 5, except that now the 47-MeV angular distribution data set is excluded when fitting the hadronic parameters.

rent. This can be inferred from comparing the resulting coupling constants in Tables I and II. The predicted angular distributions at $Q = 47$ MeV in panels (a)–(d) are now practically isotropic. They may be considered as being still compatible with the data given the experimental error bars. However, the overall results in Figs. 5 and 7 may also indicate that the COSY-11 and DISTO angular distribution data could be incompatible with each other. In this connection, it is interesting to note that the angular distribution measured recently in $pp \rightarrow pp\eta$ at $Q = 41$ MeV is completely isotropic [58]. There, the dominant η -production mechanism is the $S_{11}(1535)$ resonance current [57]. Since in the present model, the dominant η' -production mechanism is the $S_{11}(1650)$ resonance current, it is natural to expect a similar feature for the angular distribution in both reactions. Possible differences may, however, originate from the eventual difference in the excitation mechanism of these two S_{11} resonances as mentioned above. For this purpose, it would be very interesting to measure other observables, such as the invariant mass distribution, which are more sensitive to excitation mechanisms of nucleon resonances [57]. In any case, independent measurements of the angular distribution for energies $Q > 50$ MeV would help resolve the issue as far as the shape of the angular distribution is concerned.

A. Comparison to other approaches

Recently, Chiang *et al.* [35] have also investigated the $\gamma p \rightarrow p\eta'$ reaction. They concluded that the consideration of t -channel vector-meson exchanges in terms of Regge trajectories is crucial in describing the available data and that the ρ and ω meson exchanges are unable to reproduce the data. In contrast to the present work, they have not introduced a form factor at the $\eta'v\gamma$ vertex ($v = \rho, \omega$). In their calculations, the observed forward rise of the cross section is due to the interference between the Regge and the S_{11} resonance contributions. Furthermore, no need for any P_{11} resonance was found in order to describe the data. In our opinion, the application of Regge trajectories — designed for high energies and low t [59] — in the low energy regime of the SAPHIR data [30] is debatable. Moreover, such an approach cannot be used (at least not straightforwardly) in the $pp \rightarrow pp\eta'$ reaction due to the important NN FSI which has to be included in any model describing this process. This involves a loop integration for which the Regge propagator as given in Ref. [35] cannot be used. The Regge theory is a theory designed for amplitudes. Of course, with respect to our approach, one may criticize the use of a form factor at the $\eta'v\gamma$ vertex in the mesonic current, whereas we do not use any form factor at any other electromagnetic vertex. However, the use of such a form factor may be defended based on the results for the radiative decay process $\eta' \rightarrow \rho + \gamma \rightarrow \pi^+\pi^- + \gamma$. One may speculate that the relatively strong form factor needed at the $\eta'v\gamma$

vertex simulates effects of the FSI ignored in the present approach.

In any case, we have also performed the calculation of the photoproduction reaction by replacing the t -channel vector meson exchanges by the Regge trajectories following Ref. [35]. Apart from the obvious differences in the details of the treatment of the resonance current, our calculation also differs in the sign of the $\eta'\omega\gamma$ coupling constant from that employed in Ref. [35]. In the present work the signs of the $\eta'v\gamma$ couplings are inferred from a systematic analysis [43] of the pseudoscalar and vector meson radiative decays based on an $SU(3)$ Lagrangian in conjunction with the sign of the coupling constant $g_{\pi v\gamma}$ determined from a study of pion photoproduction in the 1 GeV energy region [51]. Our results using the Regge trajectories are shown in Fig. 8; the corresponding parameters are found in Table III. We see that, overall, the results are basically the same as those of Fig. 3(c) using the conventional ρ and ω meson exchanges. In particular, here also the interference between the mesonic and resonance currents is the underlying mechanism responsible for reproducing the observed angular distribution. This corroborates the findings of Ref. [35]. How-

TABLE III: Same as Table I(c), but using the exponential form factor at the electromagnetic vertices in the mesonic current (column “exp.”) and using Regge trajectories (column “Regge”).

coupling constant	exp.	Regge
Mesonic current:		
$g_{\eta'\rho\gamma}$	1.25	1.25
$g_{\eta'\omega\gamma}$	0.44	0.44
$\Lambda_M(\text{MeV})$	930	
$g_{\eta'\rho\rho}$	4.94	
$g_{\eta'\omega\omega}$	4.90	
$MNN[M = \rho, \omega]^{(\dagger)}$	Bonn	
$N^* = S_{11}$ current:		
$m_{N^*}(\text{MeV})$	1649	1932
$(g_{NN^*\gamma}g_{NN^*\eta'}, \lambda)$	(2.11, 0.90)	(0.62, 0.92)
$\Lambda_N(\text{MeV})$	1200	1200
$g_{NN^*\pi}g_{NN^*\eta'}$	0.95	
$g_{NN^*\rho}g_{NN^*\eta'}$	19.20	
$g_{NN^*\omega}g_{NN^*\eta'}$	-35.46	
$MNN[M = \pi, \rho, \omega]^{(\dagger)}$	Bonn	
$N^* = P_{11}$ current:		
$m_{N^*}(\text{MeV})$	1874	1710
$(g_{NN^*\gamma}g_{NN^*\eta'}, \lambda)$	(4.03, 0.85)	(5.93, 0.58)
$\Lambda_N(\text{MeV})$	1200	1200
$g_{NN^*\pi}g_{NN^*\eta'}$	8.91	
$g_{NN^*\rho}g_{NN^*\eta'}$	-29.44	
$g_{NN^*\omega}g_{NN^*\eta'}$	-32.26	
$MNN[M = \pi, \rho, \omega]^{(\dagger)}$	Bonn	

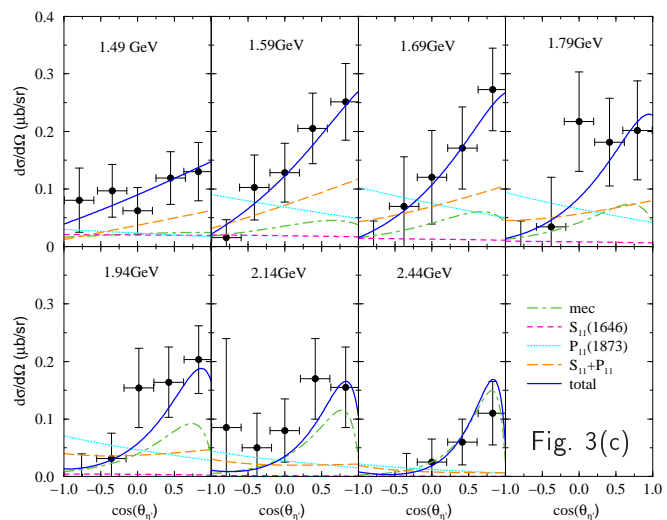
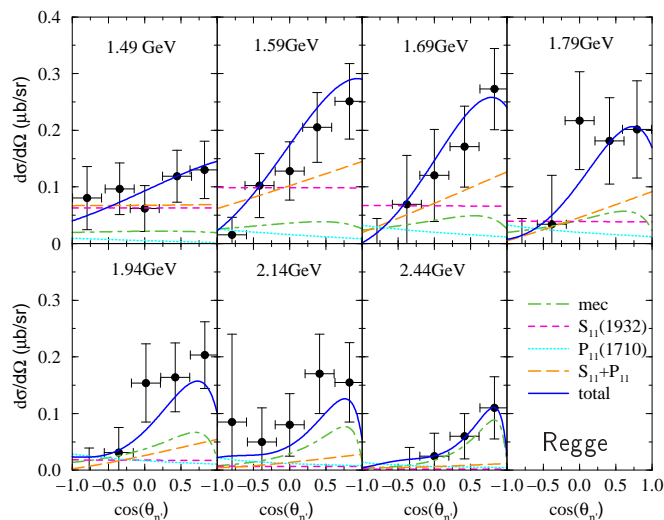


FIG. 8: (Color online) Comparison of differential cross sections for $\gamma p \rightarrow p\eta'$ using Regge trajectories (left), similar to the treatment of Ref. [35], and conventional meson-exchange currents (right) for the t -channel vector meson exchange. [The figure on the right-hand side is identical to Fig. 3(c); it is repeated here to allow for a better side-by-side comparison.]

ever, the resulting resonance masses of $m_{S_{11}} = 1932$ MeV and $m_{P_{11}} = 1710$ MeV differ considerably from those obtained in Fig. 3(c). It is natural to ask whether this discrepancy is related to the uncertainties in the determination of the resonance mass using only the cross section data as illustrated in Fig. 4 or whether it is due to different approaches used in the treatment of the t -channel exchange contribution. To address this question, in Fig. 9 we show the results of three different fits using the Regge trajectories. The solid curves are the same results shown in the left panel of Fig. 8. The dashed curves correspond to another fit resulting in the resonance masses of $(m_{S_{11}}, m_{P_{11}}) = (1932, 1950)$ MeV. One sees that the qualities of both fits are comparable to each other but the corresponding values of $m_{P_{11}}$ differ by more than 200 MeV, revealing once more (cf. Fig. 4) that the cross section data alone are insufficient to constrain accurately the resonance masses. However, we were unable to fit the data (with a comparable quality) with the mass of the S_{11} resonance much smaller than $m_{S_{11}} = 1932$ MeV. The dash-dotted curves in Fig. 9 correspond to a fit with a fixed mass of $m_{S_{11}} = 1650$ MeV. This yields a fitted mass of $m_{P_{11}} = 1811$ MeV for the P_{11} resonance. This set of the resonance masses $(m_{S_{11}}, m_{P_{11}}) = (1650, 1811)$ MeV is more in line with the set (1646, 1873) MeV obtained using the conventional vector meson exchanges in the t -channel. Here, however, the quality of the fit is inferior to that achieved in Fig. 3(c), although the data are still reproduced within their uncertainties. These considerations indicate that the determination of the resonance masses is also quite sensitive to different approaches used. Further studies of this issue are needed before a more unambiguous identification of the resonances can be made from the η' photoproduction process. It should also be noted that our calculations based on Regge trajectories

differ in details from the results obtained in Ref. [35]. As mentioned above, these differences should, in part, be due to the different treatment (in detail) of the resonance current contributions.

Sibirtsev *et al.* [36] have also reported their study of the $\gamma p \rightarrow p\eta'$ reaction quite recently. In contrast to Ref. [35] and the present work, they describe the forward rise of the angular distribution basically by the ρ and ω

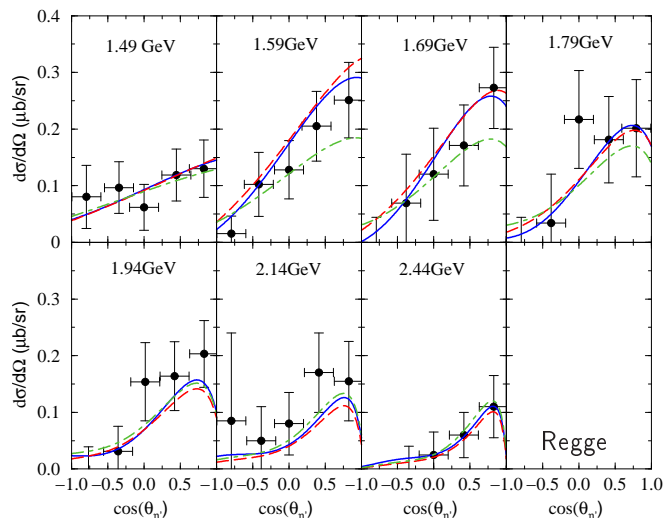


FIG. 9: (Color online) Three fits based on Regge trajectories resulting in different sets of the extracted resonance mass values. All the fits include the S_{11} and P_{11} resonances as well as the mec . The solid curves are the same ones shown in Fig. 8 with the mass values of $(m_{S_{11}}, m_{P_{11}}) = (1932, 1710)$ MeV. For the dashed curves, the corresponding mass values are (1932, 1950) MeV. The dash-dotted curves correspond to a fit with the mass values (1650, 1811) MeV.

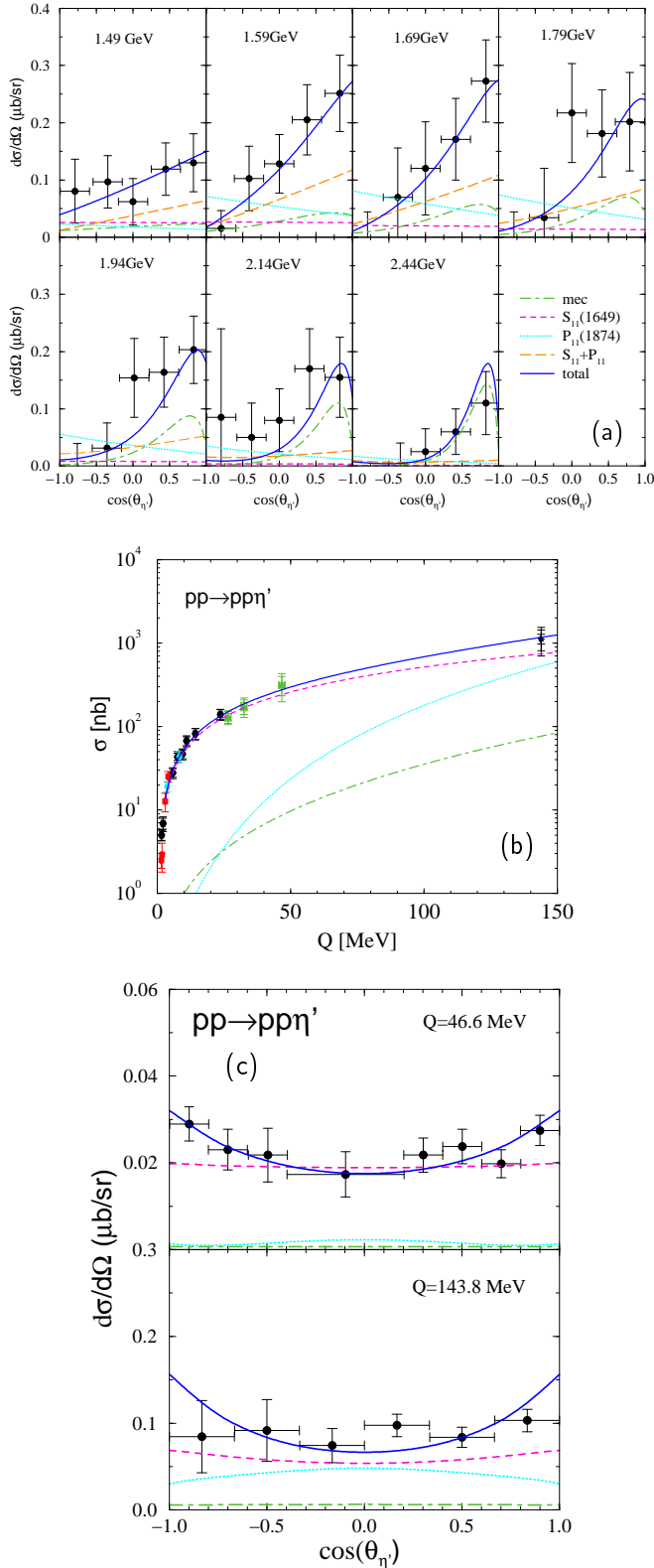


FIG. 10: (Color online) Fig. (a) here corresponds to Fig. 3(c), and (b) and (c) correspond to the two respective panels labeled (c) in Fig. 5, the difference being that now the $\gamma v\eta'$ vertex functions of dipole form [see Eq. (8)] have been replaced by exponential form factors, $F_v(t) = \exp[(t - m_v^2)/\Lambda^2]$, similar to Ref. [36] (however, with a different normalization; see text).

meson exchanges in the t -channel. They achieve this by including a (t -dependent) exponential form factor at the $\eta'v\gamma$ vertex. Moreover, the $S_{11}(1535)$ resonance was introduced in order to describe the steep rise and fall of the total cross section close to threshold. We have also repeated our calculation employing an exponential form factor at the $\eta'v\gamma$ vertex instead of the dipole form factor; the corresponding parameters are given in Table III. The results are shown in Fig. 10(a) which again exhibits the same features observed in the calculation using the dipole form factor [see Fig. 3(c)]. We were not able to reproduce their results using only the mesonic and $S_{11}(1535)$ resonance currents. The chief difference between the results shown in Fig. 10 and those in Ref. [36] is that we have used an exponential form factor normalized to unity at the on-mass-shell point $q^2 = m_v^2$, consistent with the kinematics at which the coupling constant $g_{\eta'v\gamma}$ is extracted. In Ref. [36], the form factor is normalized at $q^2 = 0$ instead. Figures 10(b) and 10(c) show the corresponding results for $pp \rightarrow pp\eta'$ using the exponential form factor. They are essentially the same as those using the dipole form factor.

The above considerations show that we arrive at the same conclusion, namely, that the interference between the meson exchange and resonance currents is the mechanism responsible for the angular distribution exhibited by the photoproduction data, irrespective of whether one uses the ρ and ω meson exchanges in the t -channel (with either dipole or exponential form factor) or Regge trajectories. Certainly, the problem of the Regge trajectory versus form factor is an extremely important issue that needs to be addressed. Judging from our findings so far, it may well be that both simulate the same physics not accounted for explicitly in these calculations.

IV. SUMMARY

We have described consistently the $\gamma p \rightarrow p\eta'$ and $pp \rightarrow pp\eta'$ reactions within an approach based on a relativistic meson-exchange model of hadronic interactions. The model includes the nucleonic and the mesonic, as well as the nucleon-resonance currents. The photoproduction process is made gauge-invariant by adding a phenomenological contact current that parametrizes the effect of the final-state interactions. The $pp \rightarrow pp\eta'$ is described within the distorted-wave Born approximation in which both the initial and final state NN interactions are taken into account explicitly.

For η' photoproduction, we have shown that the mesonic as well as the S_{11} and P_{11} resonance currents are important to describe the existing data. Our analysis, where the widths of the resonances were set to $\Gamma_{N^*} = 150$ MeV, yields a position close to 1650 MeV and 1870 MeV for the S_{11} and P_{11} resonances, respectively. This suggests that the former resonance may well be identified with the known $S_{11}(1650)$ resonance [12], whose quoted width is $\Gamma_{S_{11}} = 180$ MeV. The P_{11} reso-

nance, in contrast, does not correspond to any known resonance. It is tempting to identify it with one of the missing resonances predicted at 1880 MeV with the correspond width of $\Gamma_{P_{11}} = 155$ MeV [28, 54]. We emphasize, however, that one should be cautious with such an identification of the resonances. As we have seen, the cross section data alone do not impose enough constraints for an unambiguous determination of the resonances. To do so probably requires more exclusive data than just the cross sections. Moreover, the extracted values of the resonance masses are quite sensitive to the model used in the description of the photoproduction process. In particular, the issue of Regge trajectories versus conventional vector meson exchanges (with form factors) is of extreme importance. These points require further investigation before a conclusive identification of the resonances can be made.

Our study also shows that the nucleonic current should be relatively small. Indeed, the available photoproduction data prefer this current to be compatible with zero. In any case, the $NN\eta'$ coupling constant cannot be much larger than $g_{NN\eta'} = 3$. The η' photoproduction reaction may impose a more stringent constraint on $g_{NN\eta'}$, provided one measures the cross sections at higher energies and backward angles. In this respect, as we have also shown, spin observables such as the photon asymmetry might be suited better than the cross sections. It should be noted that the result pertaining here to the $NN\eta'$ coupling constant is, of course, a model dependent one. Indeed, what is relevant in our calculations is the product of $g_{NN\eta'}$ and the associated form factor.

We have also addressed the contradictory conclusions as to the underlying reaction mechanisms arrived in the recent work by two independent groups [35, 36]. In our consistent calculations, whether introducing a form factor at the electromagnetic vertex in the t -channel meson-exchange current or using the Regge trajectories instead, one arrives at the same conclusion; namely, the observed angular distribution is due to the interference between the t -channel and the nucleon resonance s - and u -channel contributions, irrespective of the particular approach one uses. It is conceivable, therefore, that the phenomenological aspects of the various approaches (including the present one) may be simulating the same physics not taken into account explicitly.

As for the $pp \rightarrow pp\eta'$ reaction, the present study yields

the S_{11} resonance as the dominant contribution to the production current. The P_{11} resonance, mesonic and nucleonic currents are much smaller than the S_{11} resonance current. The combined analysis of this and the photoproduction reaction was crucial for these findings. The details of the excitation mechanism of the S_{11} resonance, however, are not constrained by the currently existing data. To learn more about the relevant excitation mechanism, observables other than the cross sections, such as the invariant mass distribution, are necessary [57], in addition to measuring the $pn \rightarrow pn\eta'$ and/or $pn \rightarrow dn\eta'$ process. This process will help disentangle the isoscalar and isovector meson-exchange contributions.

The present model cannot describe the flat angular distribution in $pp \rightarrow pp\eta'$ measured by the DISTO collaboration [40] at $Q = 144$ MeV, once the recently measured angular distribution by the COSY-11 collaboration [41] at $Q = 47$ MeV is included in a global fitting for the relevant hadronic coupling parameters. The calculated result exhibits a pronounced angular dependence. If we wish, however, a flatter angular distribution at $Q = 144$ MeV — compatible with the DISTO data within the given experimental uncertainties — can be achieved provided the $Q = 47$ MeV angular distribution data is excluded from fitting. Doing so, the predicted angular distribution at $Q = 47$ MeV comes out to be nearly completely isotropic. Although this seems still compatible with the COSY-11 data, the latter exhibits some angular dependence which is too disturbing to be ignored. Independent measurements of the angular distribution for excess energies $Q > 50$ MeV will help resolve this issue.

Finally, the results of the present work should provide useful information for further investigations, both experimentally and theoretically, of the $\gamma N \rightarrow N\eta'$ and $NN \rightarrow NN\eta'$ reactions.

Acknowledgments

The authors would like to thank A. Khoukaz and the COSY-11 collaboration for providing the new COSY-11 data prior to publication. This work was supported by the COSY Grant No. 41445282 (COSY-58). The work of H. H. was supported in part by Grant No. DE-FG02-95ER-40907 of the U.S. Department of Energy.

-
- [1] J. Kogut and L. Susskind, Phys. Rev. D **10**, 3468 (1974); Phys. Rev. D **11**, 3594 (1975); E. Witten, Nucl. Phys. **B149**, 285 (1979); Ann. Phys. **128**, 363 (1980); G. 't Hooft, Phys. Rep. **142**, 357 (1986).
 - [2] S. Weinberg, Phys. Rev. D **11**, 3583 (1975).
 - [3] G. 't Hooft, Phys. Rev. Lett. **37**, 8 (1976).
 - [4] E. Witten, Nucl. Phys. **B156**, 269 (1979).
 - [5] G. Veneziano, Nucl. Phys. **B159**, 213 (1979).
 - [6] G. Christos, Phys. Rep. **116**, 251 (1984).
 - [7] T. Feldmann, P. Kroll, and B. Stech, Phys. Rev. D **58**, 114006 (1998); Phys. Lett. **B449**, 339 (1999); T. Feldmann, Int. J. Mod. Phys. **A15**, 159 (2000); T. Feldmann and P. Kroll, Phys. Scripta **T99**, 13 (2002).
 - [8] H. Leutwyler, Nucl. Phys. Proc. Suppl. **64**, 223 (1998); R. Kaiser and H. Leutwyler, Eur. Phys. J. **C17**, 623 (2000).
 - [9] T. Feldmann and P. Kroll, Eur. Phys. J. **C5**, 327 (1998).
 - [10] KLOE Collaboration, Phys. Lett. **B541**, 45 (2002).
 - [11] H. H. Jones and M. D. Scadron, Nucl. Phys. **B155**, 409

- (1979).
- [12] Particle Data Group, Eur. Phys. J. **C15**, 1 (2000).
 - [13] A. Cordier *et al.*, Nucl. Phys. **B172**, 13 (1980); S.I. Dolinsky *et al.*, Phys. Rep. **202**, 99 (1991).
 - [14] C.B. Dover and P.M. Fishbane, Phys. Rev. Lett. **64**, 3115 (1990).
 - [15] G. 't Hooft, Phys. Rev. D **14**, 3432 (1976).
 - [16] A. De Rújula, H. Georgi, and S.L. Glashow, Phys. Rev. D **12**, 147 (1975).
 - [17] P. Ball, J.-M. Frere, and M. Tytgat, Phys. Lett. **B365**, 367 (1996);
 - [18] B. Diekmann, Phys. Rep. **159**, 99 (1988); J. Jousset *et al.*, Phys. Rev. D **41**, 1389 (1990).
 - [19] B.H. Behrens *et al.*, CLEO Collaboration, Phys. Rev. Lett. **80**, 3710 (1998); T.E. Browder *et al.*, CLEO Collaboration, *ibid.* **81**, 1786 (1998).
 - [20] D. Atwood and A. Soni, Phys. Lett. **B405**, 150 (1997); Phys. Rev. Lett. **79**, 5206 (1997); W.-S. Hou and B. Tseng, *ibid.* **80**, 434 (1998); M.R. Ahmady, E. Kou, and A. Sugamoto, Phys. Rev. D **58**, 14015 (1998); E. Kou, *ibid.* **63**, 054027 (2001).
 - [21] S.D. Bass, Phys. Lett. **B463**, 286 (1999).
 - [22] J. Ashman *et al.*, Phys. Lett. **B206**, 364 (1988).
 - [23] G.M. Shore and G. Veneziano, Nucl. Phys. **B381**, 23 (1992).
 - [24] T. Hatsuda, Nucl. Phys. **B329**, 376 (1990); A.V. Efremov, J. Soffer, and N. A. Törnqvist, Phys. Rev. Lett. **64**, 1495 (1990); Phys. Rev. D **44**, 1369 (1991).
 - [25] G.M. Shore and G. Veneziano, Phys. Lett. **B244**, 75 (1990).
 - [26] S. Okubo, Phys. Lett. **5**, 165 (1963); G. Zweig, CERN Report No. TH412, 1964; J. Iizuka, Prog. Theor. Phys. Suppl. **37-38**, 21 (1966).
 - [27] G. Altarelli and G.G. Ross, Phys. Lett. **B212**, 391 (1988); R.D. Carlitz, J. C. Collins, and A. H. Müller, *ibid.* **B214**, 229 (1988).
 - [28] S. Capstick and N. Isgur, Phys. Rev. D **34**, 2809 (1986); S. Capstick and W. Roberts, *ibid.* **47**, 1994 (1993); **49**, 4570 (1994); **57**, 4301 (1998); **58**, 074011 (1998).
 - [29] ABBHHM Collaboration, Phys. Rev. **175**, 1669 (1968); Nucl. Phys. **B108**, 45 (1976).
 - [30] R. Plötzke *et al.*, Phys. Lett. **B444**, 555 (1998); J. Barth *et al.*, Nucl. Phys. **A691**, 374c (2001).
 - [31] J.F. Zhang, N.C. Mukhopadhyay, and M. Benmerrouche, Phys. Rev. C **52**, 1134 (1995).
 - [32] Z. P. Li, J. Phys. **G23**, 1127 (1997).
 - [33] B. Borasoy, Eur. Phys. J. **A9**, 95 (2000).
 - [34] Q. Zhao, Phys. Rev. C **63**, 035205 (2001).
 - [35] W. T. Chiang, S. N. Yang, L. Tiator, M. Vanderhaeghen, and D. Drechsel, Phys. Rev. C **68**, 045202 (2003).
 - [36] A. Sibirtsev, Ch. Elster, S. Krewald, and J. Speth, nucl-th/0303044.
 - [37] M. Dugger, Ph.D. thesis, Arizona State University, 2001; approved JLab Hall-B Experiment E-91-008 (B.R. Ritchie, Spokesperson; see http://www.jlab.org/exp_prog/generated/apphallb.html).
 - [38] Crystal Barrel Collaboration (see <http://www.cb.uni-bonn.de/>).
 - [39] F. Hibou *et al.*, Phys. Lett. **B438**, 41 (1998); P. Moskal *et al.*, Phys. Rev. Lett. **80**, 3202 (1998); P. Moskal *et al.*, Phys. Lett. **B474**, 416 (2000); P. Moskal *et al.*, *ibid.* **B482**, 356 (2000).
 - [40] F. Balestra *et al.*, Phys. Lett. **B491**, 29 (2000).
 - [41] A. Khoukaz *et al.*, COSY-11 Collaboration, nucl-ex/0401011.
 - [42] A. Sibirtsev and W. Cassing, Eur. Phys. J. **A2**, 333 (1998); V. Bernard, N. Kaiser, and U. Meißner, *ibid.* **A4**, 259 (1999); E. Gedalin, A. Moalem, and L. Razdolskaja, Nucl. Phys. **A650**, 471 (1999); V. Baru, J. Haidenbauer, C. Hanhart, A. Kudryavtsev, and J. Speth, Eur. Phys. J. **A6**, 445 (1999).
 - [43] K. Nakayama, H.F. Arellano, J.W. Durso, and J. Speth, Phys. Rev. C **61**, 024001 (1999).
 - [44] B.C. Pearce and I.R. Afnan, Phys. Rev. C **34**, 991 (1986).
 - [45] H. Haberzettl, Phys. Rev. C **56**, 2041 (1997).
 - [46] H. Haberzettl, C. Bennhold, T. Mart, and T. Feuster, Phys. Rev. C **58**, R40 (1998).
 - [47] R.M. Davidson and R. Workman, Phys. Rev. C **63**, 025210 (2001).
 - [48] K. Nakayama, J. Speth, and T.-S.H. Lee, Phys. Rev. C **65**, 045210 (2002).
 - [49] Ch. Hanhart and K. Nakayama, Phys. Lett. **B454**, 176 (1999).
 - [50] R. Machleidt, Adv. Nucl. Phys. **19**, 189 (1999).
 - [51] H. Garcilazo and E. Moya del Guerra, Nucl. Phys. **A562**, 521 (1993).
 - [52] K. Nakayama, A. Szczurek, C. Hanhart, J. Haidenbauer, and J. Speth, Phys. Rev. C **57**, 1580 (1998).
 - [53] G. Höhler, πN Newsletter **14**, 168 (1998).
 - [54] S. Capstick *et al.*, Phys. Rev. C **59**, R3002 (1999).
 - [55] M. Batinić *et al.*, Phys. Rev. C **51**, 2310 (1995); *ibid.* **57**, 1004 (1998).
 - [56] W. Grein and P. Kroll, Nucl. Phys. **A338**, 332 (1980).
 - [57] K. Nakayama, J. Haidenbauer, C. Hanhart, and J. Speth, Phys. Rev. C **68**, 045201 (2003).
 - [58] M. Abdel-Bary *et al.*, Eur. Phys. J. **A 16** 127 (2003).
 - [59] See, e.g., J.K. Storrow, in “*Electromagnetic Interactions of Hadrons*”, edited by A. Donnachie, and G. Shaw, (Plenum Press, 1978), Vol. I, p. 263.